

# Impact of Planetary Boundary Layer Assumptions on HWRF Forecast Skill: Final Report

Robert G. Fovell

Department of Atmospheric and Environmental Sciences  
University at Albany, State University of New York  
rfovell@albany.edu

*Executive summary:* Two PBL schemes, YSU and MYNN, have been modified to work with HWRF's NMM-based core and its GFDL surface layer scheme. YSU was selected owing to its shared lineage with the operational HWRF scheme (GFS and GFSEDMF) and its tendency to produce markedly different results with respect to mixing strength and depth and its consequent impact on storm radial width. MYNN, specifically MYNN2, is a TKE-based scheme that is a more complete implementation of Mellor and Yamada than the MYJ parameterization. MYNN was selected owing to favorable results obtained in experiments using the WRF-ARW core. Semi-idealized simulations, designed to closely follow the operational configuration, were made using these and other schemes and physics combinations. Comparisons with observations including eddy mixing and inflow profile estimates suggest that MYNN2 has promise with respect to modeling the hurricane boundary layer and should be considered for operational use, with the understanding that other model physics that directly or indirectly interacts with PBL mixing may also need to be reevaluated or revised.

## 1. Background

Our past work identified areas for improvement in the operational Hurricane Weather Research and Forecasting (HWRF) model that have contributed to its increasing skill in forecasting the track, intensity and structure of tropical cyclones (TCs). Specifically, we identified issues with the HWRF model's radiation scheme (originating at GFDL), and explained how and why cloud-radiative forcing (CRF) that was missing in the scheme directly and indirectly influences TC structure and size (Bu et al. 2014; Fovell et al. 2016). For our 2013 DTC project, we studied the results of the DTC's radiation and microphysics experiment of retrospective cases to understand why a CRF-enabled radiation scheme (RRTMG) and a more sophisticated microphysics parameterization (Thompson) combined to degrade forecast skill. This led us to explore the role of planetary boundary layer (PBL) mixing in determining storm size, which was the subject of (Bu et al. 2017).

The CRF and PBL studies show how physical parameterizations can cooperate and compete in a complex numerical model. Other factors being equal, the longwave warming component of CRF results in storm expansion by encouraging gentle but persistent ascent above the boundary layer, resulting in more radially extensive convective activity (Bu et al. 2014; Fovell et al. 2016). However, vertical mixing of moisture in the PBL can accomplish the same thing (Bu et al. 2017). Our analysis showed that the lack of CRF in the operational HWRF model was being compensated

by ostensibly excessive vertical mixing in the PBL scheme, such that when the CRF issue was fixed the model TCs acquired a positive size bias (Bu 2015; Bu and Fovell 2015; Bu et al. 2017). This was particularly apparent in the Atlantic basin in the DTC’s retrospective examination of 2012 storms.

Our approach to studying model physics and physics interactions has involved detailed composite analyses of not only individual TCs from retrospective cases but also what we term “semi-idealized” simulations, as introduced in Fovell and Su (2007). Semi-idealized simulations employ operational models and configurations but with simplified initial conditions constructed from a single tropical sounding. Often, we take the base state environment to be calm and horizontally homogeneous, with constant sea surface temperature, but this is not required and easily altered (e.g., Hsu et al. 2013; Nava et al. 2014). Into this environment, a bogussed vortex or a virtual temperature perturbation (Cao et al. 2011) is inserted, the latter leading to the organic development of a TC over the course of about one simulated day.

Comparison of semi-idealized simulations from different models can be very revealing. As an example, it was intercomparisons of HWRF simulations with versions created using the Advanced Research WRF (ARW) core that helped reveal the CRF issue in the GFDL radiation scheme. This helped explain some (and by no means all; see below) of the dramatic differences seen with respect to TC structure between the two versions of WRF. In the case of HWRF, we have been integrating the semi-idealized model without ocean model coupling for simplicity, although this also is not a requirement.

## 2. Motivation

The literature demonstrating the importance of PBL schemes on hurricanes is sizable; a few recent contributions include Braun and Tao (2000), Nolan et al. (2009a), Nolan et al. (2009b), Hill and Lackmann (2009), Smith and Thomsen (2010), and Kepert (2012). With respect to the HWRF model, it has been realized for some time that the longstanding default HWRF boundary layer scheme, the GFS PBL, has serious deficiencies (Gopalakrishnan et al. 2013). However, other available parameterizations had not been very well explored. As a consequence, we proposed to assess the sensitivity of HWRF model storms, especially with respect to structure and radial width, to PBL treatments.

The GFS PBL scheme originated in the old MRF model (Hong and Pan 1996), and descended from Troen and Mahrt (1986) and that study’s predecessors. It is a  $K$ -profile parameterization scheme that imposes a parabolic profile of eddy momentum diffusivity ( $K_m$ ) between the surface and the top of the PBL, and combines this with a countergradient term to represent deep-layer mixing in the convective boundary layer. Computation of the PBL height  $h$  depends on the specification of a critical bulk Richardson number,  $\text{Rib}_{cr}$ , with larger values of  $\text{Rib}_{cr}$  resulting in greater PBL depths. In recent versions of the scheme, different  $\text{Rib}_{cr}$  values may be specified over ocean and land (`coef_ric_s` and `coef_ric_l`) and also modified by the surface Rossby number if the `var_ric` option is selected. Over ocean surfaces, the operational model has been selecting  $\text{Rib}_{cr}$

= `coef_ric_s` = 0.25.

Given PBL depth  $h$ , the vertical profile of eddy momentum diffusivity  $K_m$  within the PBL is computed using

$$K_m = k(u_*/\phi_m)Z \left[ \alpha \left( 1 - \frac{Z}{h} \right)^2 \right], \quad (1)$$

where  $k$  is the von Karman constant (=0.4),  $u_*$  is the friction velocity,  $\phi_m$  is the wind profile function evaluated at the top of the surface layer, and  $Z$  is the height above the surface ( $0 \leq Z \leq h$ )<sup>1</sup>. The  $\alpha$  parameter (Gopalakrishnan et al. 2013), representing a number between 0 and 1, was added to (1) in the 2012 version of HWRF, motivated by the PBL and eddy mixing observations of Zhang et al. (2011a). This parameter was designed to prevent the development of unrealistically large mixing in the hurricane inner core that, owing to (1), is a necessary consequence of large diagnosed PBL depth. Figure 1 shows HWRF mixing (grey dots) compared to Zhang et al. (2011a) observations (purple crosses) when  $\alpha$  was set to 0.25. In operational practice, however, larger values of this parameter were adopted.

Equation (1) is only used within the diagnosed PBL. In the free atmosphere,  $K_m$  is computed as a function of the vertical shear, a height-dependent mixing length scale, and a stability function dependent on the gradient Richardson number (cf. Hong 2010; Louis 1979), essentially a first-order treatment.

Figures 2 and 3 show temporally- and azimuthally-averaged profiles of  $K_m$  and 10-m wind speed from semi-idealized simulations as a function of  $\alpha$  (Bu et al. 2017), all computed in a vortex-following fashion during the final 24 h of 96 h simulations. Left unconstrained (i.e.,  $\alpha = 1.0$  in Fig. 2), the GFS scheme yields relatively large mixing maximized about 500 m above mean sea level (MSL). Lowering  $\alpha$  reduces the mixing substantially, but without affecting the fundamental shape or PBL depth very much. The  $\alpha$  parameter has a sizable impact on the amount of mixing being applied to momentum and heat within the PBL and this strongly modulates storm inflow, structure, and width. Note that as  $\alpha$  is decreased, storm width (as indicated, for example, by the 34-kt wind radius, or R34) decreases substantially (Fig. 3). At the same time, the low-level inflow becomes much stronger and shallower (Fig. 4), consistent with the findings of Gopalakrishnan et al. (2013).

For the 2015 operational model, we provided an algorithm (Fovell and Bu 2015; Bu 2015) for the GFS PBL scheme that limited  $K_m$  in the presence of high wind speeds based on the Zhang et al. (2011a) data that would not be applied over land and over water would not likely to be activated beyond the hurricane inner core. This ‘‘Capped  $K_m$ ’’ approach removed  $\alpha$  as an adjustable, external parameter (see grey curve on Fig. 2) but also obviously did not directly affect PBL depth. It is noted that the modification of Gopalakrishnan et al. (2013) and this  $K_m$  capping both create an inconsistency with respect to the surface layer that was identified and mitigated by Wang et al. (2018). Also, since 2015, a windspeed dependency was added to  $\text{Rib}_{cr}$  based on Vickers and Mahrt

---

<sup>1</sup>Eddy mixing applied to temperature and scalars,  $K_h$ , may not be identical to  $K_m$ . This is scheme-dependent and ignored for simplicity herein. Furthermore, it is noted YSU’s treatment of the first parenthetical term is more complex than GFS or GFSEDMF’s.

(2004) and the operational HWRF has shifted to the GFSEDMF scheme, which differs from its predecessor primarily by its handling of countergradient mixing. A modified version of the  $K_m$  cap was implemented in this revised version.

Figure 2 also shows the  $K_m$  profile obtained when the YSU scheme was used (black curve). YSU is a not-uncommon selection for TC modeling with WRF-ARW, which makes it an obvious choice for comparisons, and for these experiments we used the surface layer scheme usually employed in ARW. While also descended from Troen-Mahrt and the MRF scheme, YSU obviously resulted in both much shallower and weaker mixing, these being strongly related owing to (1). As shown in Bu et al. (2017), the reduction of mixing, especially that applied to water vapor, can result in a substantially narrower storm (Fig. 3). Bu et al. (2017) explained that vertical mixing of moisture beyond the inner core enhanced the likelihood of convective activity, which works to broaden the radial extent of the cyclonic winds.

There are a number of potentially important differences between GFS and YSU, but one of the most influential is the selection of the critical Richardson number when the surface layer is unstable. As noted above, HWRF’s PBL scheme uses  $\text{Rib}_{cr} = 0.25$  over water surfaces but YSU has adopted  $\text{Rib}_{cr} = 0.0$  for the unstable case since Hong (2010). In *theory*, YSU’s reduced  $\text{Rib}_{cr}$  was designed to accommodate the addition of explicit PBL top entrainment to the scheme, but in *practice* – at least with respect to TCs – it has a profound and potentially important impact on the wind field near and above the surface.

### 3. Model modifications

The findings discussed above motivated this proposed work to DTC. This project ultimately involved modifying *two* PBL schemes – YSU and MYNN2 – to work more properly and competitively with the operational HWRF system. These were implemented into recent versions of WRF, including ARW, and tested and compared to the GFS and GFSEDMF parameterizations using semi-idealized simulations. MYNN (Nakanishi and Niino 2004) is a turbulent kinetic energy (TKE) scheme which shared a common origin (Mellor and Yamada 1974) with the Mellor-Yamada-Janjic (MYJ) option (Janjić 1994). To be competitive, and to reduce sources of variation among the experiments, the schemes had to make use of the GFDL surface layer code, which has been heavily modified over time focusing on tropical cyclones in general and HWRF performance in particular.

For YSU, the modifications included:

- Establishing compatibility with the GFDL surface layer scheme;
- Adding new capabilities for controlling details of the YSU parameterization;

Primary modifications were made to the NMM Registry, PBL driver (`module_pbl_driver.F`), the HWRF solver and model physics driver (`solve_nmm.F` and `module_PHYSICS_CALLS.F`) as well as the PBL codes themselves (`module_bl_ysu.F`, `module_bl_gfs.F`, and `module_bl_gfsedmf.F`). Other

changes had to be made to get the schemes working properly, and parallel modifications were made to ARW to preserve compatibility.

The new capabilities involved switches affecting some of the more important differences between the YSU and GFS/GFSEDMF codes. These included controlling the activation of countergradient mixing applied to scalars (`ysu_cgrad_scalar`) and momentum (`ysu_cgrad_mom`), the critical bulk Richardson number  $Rib_{cr}$  for the unstable case (`ysu_br_cr_ub`), and a switch that devolved YSU into a 1st order scheme (`ysu_firstorder`) like Louis (1979) that was motivated by Kepert (2012). As noted above, HWRF’s GFS PBL used a larger  $Rib_{cr}$  and also did not subject momentum to countergradient mixing. It is noted the GFSEDMF scheme utilizes a different (mass flux) approach to countergradient mixing, which is applied to both momentum and scalars.

MYNN was not included in our original proposal, but was explored owing to favorable comparisons with observations in the ARW version of our semi-idealized tests (and marked deficiencies that emerged from those same tests with YSU). The modifications required for MYNN were much more extensive and the implementation is not yet 100% complete at this writing. The primary challenges were:

- Getting MYNN working with the NMM core;
- Getting MYNN to operate with the GFDL surface layer scheme;

The former required extensive modification of `Registry.NMM`, the MYNN code (`module_bl_mynn.F` and `module_sf_mynn.F`), the surface layer driver (`module_surface_driver.F`) and further revisions of other previously modified codes. MYNN’s EDMF option calls for vertical motion but this is set to zero in the present version. Some as yet unimplemented features include stochastic perturbations and the level 3 version of the parameterization.

All of our code modifications have been provided to DTC, were tested, and have been incorporated into the HWRF code trunk.

## 4. Experiments

Semi-idealized experiments along the lines of Bu et al. (2014) and Bu et al. (2017) were designed. The simulations specifically described herein mostly employed the 2018 version of HWRF (V3.9.1.1) using a nearly-identical domain configuration to that used operationally in the 2018 hurricane season (“H218”). This consisted of three telescoping domains (390x780 for the outermost domain with nests being 268x538), with resolutions of about 13.2, 4.4, and 1.4 km, and 75 vertical levels at specified locations. Note both the horizontal and vertical resolution are higher than in Bu et al. (2017).

Operational physics selections other than PBL scheme were retained, including the latest cumulus scheme, except that both standard (Ferrier-Aligo) and Thompson microphysics were considered. Only simulations employing the latter are included in this report. Operational settings for options controlling horizontal mixing (`coac`), surface exchange coefficients (`icoef_sf`), and cloud-radiation

effects (`icloud`) were also adopted. However, the physics time stepping (`nphs`) varies among our experiments, as explained below.

As before, the simulations were 96 h in length and commenced with a synoptic-scale virtual temperature perturbation that, with the help of a cumulus parameterization, can form a circulation of tropical storm intensity within 24 h. At the 24 h mark, the cumulus scheme in the innermost domain (D3) was deactivated<sup>2</sup>. Physics options held fixed for the runs shown include the Thompson microphysics scheme and RRTMG radiation. Our primary focus is again on the final 24-h period (Fig. 5).

The PBL/surface layer schemes specifically examined herein include

- GFSEDMF with the Fovell-Bu mixing cap and GFDL surface layer (i.e., the operational configuration);
- GFSEDMF/GFDL without the mixing cap;
- YSU with GFDL surface layer (implemented for this project);
- MYJ with the MYJ surface layer scheme;
- MYNN with the GFDL surface layer (implemented for this project);

The critical contribution of the GFDL surface layer scheme cannot be discounted. In sharp contrast with our experience with WRF-ARW, HWRF simulations that do NOT use the GFDL surface layer scheme are typically unrealistically weak, given the favorable environmental conditions provided in these tests.

Some simulations differ from the operational approach with respect to the physics time stepping (`nphs`) strategy. The 2018 operational model uses `nphs` = 2,6,6, which means the outermost domain calls model physics every other time step, and the nests doing so every 6th step. This contrasts with the ARW standard practice, which does not skip time steps, at least for PBL physics. Figure 6 contrasts time series of domain maximum 10-m wind (kts) from simulations using the operational `nphs` selection with those calling physics every step. For both PBL schemes, the model TCs develop faster with more frequent physics calls. For YSU (Fig. 6a), the model reaches a reasonably steady state prior to 72 h, the start of the temporal averaging period. For this reason, YSU simulations included herein employ the operational setting. This is not generally true for MYNN (Fig. 6b), so physics is called every step when that scheme is used. It should be kept in mind that MYNN results may be disadvantaged by the longer physics time steps employed operationally.

## 5. Basic results

First, we assess the primary role of the critical Richardson number,  $Rib_{cr}$ , on the mixing strength and depth, using simulations made using H217 and the GFS scheme in place of GFSEDMF. Figure

---

<sup>2</sup>The cumulus scheme has been modified to be scale-aware, and experiments retaining the cumulus scheme with D3 were also made, but are not discussed herein.

7 demonstrates the change of mixing strength and depth obtained when varying  $\text{Rib}_{cr}$  from the schemes' default values. Keeping in mind that PBL depth and maximum mixing strength and height are not independent owing to (1), we see that decreasing  $\text{Rib}_{cr}$  with GFS from its default value towards YSU's results in weaker mixing concentrated closer to the surface, and increasing YSU's critical value brings about results more comparable to the standard GFS. As could be expected, varying  $\text{Rib}_{cr}$  in the GFS scheme has a comparable impact on inflow depth and strength as varying  $\alpha$ , as illustrated by Fig. 8.

This makes the specification of  $\text{Rib}_{cr}$  in these schemes very important. As noted above, the original intent of reducing  $\text{Rib}_{cr}$  in the YSU scheme was not to bring about a very substantial reduction in the depth of the convective mixed layer, so this is an unintended result. The fundamental problem is that  $\text{Rib}_{cr}$  may be an inappropriate criterion for determining boundary layer depth as discussed in Zhang et al. (2011b) and, if so, this may suggest that the  $K$ -profile approach is not very suitable for the TC environment.

Now we shift to the H218 code and configuration and replace GFS with the GFSEDMF parameterization. Figure 9 shows the effect of PBL scheme on radial inflow and eddy mixing  $K_m$ . These plots focus on the lower troposphere, as in Figs. 4 and 7, but horizontal axis extends to five times the radius of maximum wind (5RMW) and the inflow velocities are scaled relative to the each run's maximum value, which is reported at the top right of each panel. The MYJ scheme uses its own surface layer scheme (MYJSFC) while the others utilize GFDL.

The unconstrained GFSEDMF (Fig. 9a) generates large mixing spread over a deep and wide area, along with very deep (and relatively weak) inflow. Capping the mixing clearly reduces the magnitude of the mixing but not the depth or radial extent (Fig. 9b). However, this storm's inflow is considerably stronger and more concentrated near the surface, and the inflow layer depth (1.2 km) is roughly constant with radius between 2-5RMW.

Compared to the capped GFSEDMF, the much shallower and weaker mixing produced by YSU with GFDL (Fig. 9c) does not change the maximum inflow much but results in larger vertical and horizontal shear. Note the outflow produced above the inflow layer is more prominent. Deepening the mixing in YSU via increasing  $\text{Rib}_{cr}$  (Fig. 9d) spreads the inflow over a larger depth. Ostensibly, MYJ produces results rather comparable to the default YSU (Fig. 9e).

The MYNN scheme (Fig. 9f) produces the most distinctly different result, in several respects. Like YSU and MYJ, the mixing at larger radii is not necessarily smaller than capped GFSEDMF, but is concentrated closer to the sea surface. However, closer to the RMW, the mixing is larger and extends to a greater depth, being more comparable to the capped GFSEDMF and might be expected from the shear and reduced stability present there (Kepert 2012; Kepert et al. 2016). This combination results in a particularly strong inflow near the RMW (26 m/s) beneath a well-formed outflow layer.

## 6. Observational comparisons

In this section, we compare the semi-idealized simulations to observations drawn from Zhang et al. (2011a) and Zhang et al. (2011b). In particular, as previously introduced in Fig. 1, Zhang et al. (2011a) estimated  $K_m$  near 500 m MSL from aircraft data. They found that mixing generally increased with wind speed at this level, albeit with some substantial scatter. A subset of their data (removing estimates marked on Fig. 1) are shown in Fig. 10 as black dots.

Without capping (Fig. 10a), the GFSEDMF scheme generates mixing that far exceeds the Zhang et al. (2011a) estimates at nearly all wind speeds. This is not only true for the azimuthally averaged comparisons (red dots) but also for all points located at 500 m MSL (grey dots). This was the motivation for the Gopalakrishnan et al. (2013)  $\alpha$  modification of (1) and the cap fashioned by Fovell and Bu (2015) and Bu and Fovell (2015). The cap scales the mixing produced by the GFS and GFSEDMF schemes such that the magnitude at 500 m MSL does not exceed the wind speed (in m/s) divided by 0.6 at 500 m MSL, a relationship suggested by the Zhang et al. (2011a) estimates and indicated in Fig. 1. In theory, PBL mixing is permitted to be smaller than the capped value, but in practice the GFSEDMF is so diffusive that mixing at this level varies little from the enforced maximum (Fig. 10b).

We saw the YSU scheme with the default critical Richardson number produces relatively small mixing concentrated close to the sea surface. The depth that  $\text{Rib}_{cr} = 0$  produces is so shallow that little mixing extends above the 500 m level (Fig. 9c). As a consequence, high wind speeds at this level are associated with very small diffusion values (Fig. 10c). It is stipulated that there are only two points for wind speeds exceeding 40 m/s in the Zhang data subset, but it remains we suspect that the diffusion generated by the default YSU scheme (and MYJ as well; Fig. 10e) is unrealistically low. Indeed, increasing the YSU's  $\text{Rib}_{cr}$  slightly, to 0.0125, deepens the mixing layer sufficiently that the diffusion generated at 500 m MSL becomes much more comparable with the Zhang estimates (Fig. 10d). Taken in isolation, this might suggest that a small adjustment to YSU could obviate the essentially artificial adjustments needed by GFSEDMF to produce realistic mixing. Still, we will soon see that this version of YSU fails to generate reasonable vertical profiles of inflow based on the Zhang et al. (2011b) composites.

Encouragingly, MYNN does a particularly good job of matching the observationally-derived  $K_m$  estimates (Fig. 10f) across the available wind speed range at 500 m MSL, and does so without modification or artificial constraints. This brings us to the second comparison, based on Fig. 10 from Zhang et al. (2011b).

Zhang et al. (2011b) provided estimates of radial inflow velocity as a function of radius and height for different TC strengths. Figure 11 shows the composite created for the category 4 and 5 cases. Inflow has been scaled relative to the maximum value of 25.5 m/s, which occurred just above the sea surface at about the radius of maximum wind. From this composite, a vertical profile of maximum scaled inflow was created by identifying the largest radial inflow between 1-2RMW at each height. This profile is shown in Fig. 12 as the black line.

For comparison, vertical maximum inflow profiles were also constructed from the simulations.

These identified the fastest inbound speeds from the storm center out to about 4RMW from the temporally- and azimuthally-averaged winds at each model level. As suggested by Fig. 9, however, the maximum value was invariably located between 1 and 2 multiples of the RMW.

For GFSEDMF, (Fig. 12a, blue solid curve), it is clear that the capped version follows the observed profile rather closely, at least below 1.25 km. As the maximum inflow speed (24 m/s, see Fig. 9b) was also comparable to the Cat. 4-5 composite, both the dimensional winds and vertical shear are well-captured in this simulation. Without capping, however, inflow is both too weak (13 m/s, Fig. 9a) and has too little vertical shear (Fig. 12a, blue dashed curve). Thus, we can conclude that the capped GFSEDMF/GFDL model physics compares well with both the inflow and  $K_m$  observations, but requires a very strong and quite artificial restriction to attain this favorable result.

YSU with the default  $\text{Rib}_{cr}$  of zero for the unstable PBL follows the observed maximum inflow profile even more closely (Fig. 12b, red solid curve). However, recall that the  $K_m$  comparison suggested that its mixing is too shallow, or at least too weak at 500m MSL (Fig. 10), and very similar results are obtained with MYJ (Figs. 10e and 12c). Increasing the critical Richardson number slightly resulted in a more favorable comparison with the mixing estimates but at the cost of weakened inflow (Fig. 9d) and reduced shear (Fig. 12b, blue dashed curve). Thus, simply revising YSU to employ a larger  $\text{Rib}_{cr}$  does not appear to be warranted.

In contrast, MYNN achieved high consistency with both the vertical inflow profile and the mixing estimates (Figs. 10f and 12a). This is an encouraging result, one which suggests that MYNN may be somewhat “less wrong” than other PBL parameterizations, or at least may be more naturally adaptable to the hurricane boundary layer. These simulations were made without implementing the mass flux component for accomplishing non-local mixing. Full implementation of that component of the parameterization has not yet been accomplished.

## 7. Above and beyond the inner core PBL

We have seen that PBL schemes can substantially influence the radial size of TCs, owing in part to its vertical mixing of water vapor (Bu et al. 2017). However, in these experiments, the operational (capped) GFSEDMF and MYNN schemes have produced very similar wind profiles, at least in the inner core near the surface, both being substantially narrower than the uncapped version of GFSEDMF. This can also be seen in Fig. 13. The large circles indicate the 34-kt wind radii.

Some potentially important differences emerge farther above and also beyond the inner core, however. First, note that the tangential wind field is a fair bit wider in the capped GFSEDMF storm compared to the MYNN (Fig. 14) for the relatively weaker winds found at larger radii. This is a logical consequence of the more vigorous mixing produced by the GFSEDMF beyond the inner core. In Fig. 15, note that the MYNN mixing is concentrated closer to the sea surface beyond about 100 km from the storm center. As a consequence of its larger mixing, the GFSEDMF storm is more moist above about 900 m MSL (Fig. 15c). This has a consequence for outer convective

activity (Fig. 16), which is somewhat larger with the currently operational PBL physics.

## 8. Retrospective cases

After providing updated model code to accommodate YSU with the GFDL surface layer, EMC conducted retrospective simulations to assess the impact of adopting YSU on forecast skill. As a consequence of this testing, YSU was not selected for the operational configuration in 2018. Both EMC and DTC have been conducting simulations of past cases to determine if MYNN positively influences skill. This testing is incomplete at this writing, but preliminary results suggested that while MYNN was performing well, it was contributing to a small positive size bias. Semi-idealized testing has suggested that, other factors being equal, activating the (still not completely implemented) mass flux component of MYNN can mitigate this positive bias. This suggestion was passed on to EMC and DTC.

## 9. Discussion and conclusions

This work began with a recognition that vertical eddy mixing was likely excessive in HWRF's GFS and GFSEDMF PBL parameterizations and that alternatives not requiring artificial constraints should be investigated. We started with the YSU option because this parameterization is frequently employed with WRF-ARW, and shares a similar lineage with the HWRF GFS and GFSEDMF schemes, but naturally results in weaker mixing that is also concentrated rather closer to the sea surface (Bu et al. 2017). Comparisons with available observations, at this time consisting of eddy mixing estimates from Zhang et al. (2011a) and vertical inflow profiles from Zhang et al. (2011b), have suggested that while its inflow profiles appeared reasonable, the mixing generated by YSU may be too weak and/or concentrated too close to the sea surface. This might ostensibly be addressable by deepening the convective boundary layer, by adopting a slightly larger critical Richardson number,  $Rib_{cr}$ . However, while this makes the YSU results more consistent with the limited diffusion information, it results in inflow that is too weak and possesses too little vertical shear relative to the observations.

In contrast, the MYNN scheme (specifically, MYNN2), produced results in the semi-idealized testing that were congruent with both the inflow and mixing data. This scheme is currently being assessed further using retrospective simulations. Most of our testing was performed without implementing the relatively recent mass flux component, which is a parameterization for non-local mixing. Limited testing with the mass flux scheme, which has not yet been fully adapted to HWRF's NMM core, has suggested that it may address a positive storm size bias that was emerging from preliminary testing. However, even if MYNN and/or the operational schemes are producing acceptable wind fields at the 10 m MSL level, our semi-idealized testing has suggested that systematic differences may occur aloft, where fewer validating observations are available.

Future work should focus on understanding why MYNN is outperforming MYJ, as both are versions of the Mellor and Yamada model. While MYNN represents a more complete implementa-

tion of Mellor-Yamada, the differences between these parameterizations may reside in the values for various coefficients adopted in the respective codes. Understanding these sensitivities may result in an even more skillful parameterization for tropical cyclone applications.

## REFERENCES

- Braun, S. A. and W.-K. Tao, 2000: Sensitivity of high-resolution simulations of Hurricane Bob (1991) to planetary boundary layer parameterizations. *Mon. Wea. Rev.*, **128**, 3941–3961.
- Bu, Y., 2015: Influence of cloud-radiative forcing and the planetary boundary layer on tropical cyclone structure. Ph.D. thesis, University of California, Los Angeles, 107 pp., Los Angeles, California, USA.
- Bu, Y. P. and R. G. Fovell, 2015: Model physics influences on tropical cyclone size. *16th Conf. on Mesoscale Processes*, American Meteorological Society.
- Bu, Y. P., R. G. Fovell, and K. L. Corbosiero, 2014: Influence of cloud-radiative forcing on tropical cyclone structure. *J. Atmos. Sci.*, **71**, 1644–1662, doi:10.1175/JAS-D-13-0265.1.
- Bu, Y. P., R. G. Fovell, and K. L. Corbosiero, 2017: The influences of pounary layer mixing and cloud-radiative forcing on tropical cyclone size. *J. Atmos. Sci.*, **74**, 1273–1292, doi:10.1175/JAS-D-16-0231.1.
- Cao, Y., R. G. Fovell, and K. L. Corbosiero, 2011: Tropical cyclone track and structure sensitivity to initialization in idealized simulations: A preliminary study. *Terrestrial, Atmospheric and Oceanic Sciences*, **22**, 559–578, doi:10.3319/TAO.2011.05.12.01(TM)1.
- Fovell, R. G. and Y. P. Bu, 2015: Improving HWRF track and intensity forecasts via model physics evaluation and tuning. Dtc visitor program final report, Developmental Testbed Center, 28 pp. URL [http://www.dtcenter.org/visitors/reports\\_2013/DTC\\_report\\_2013\\_Fovell.pdf](http://www.dtcenter.org/visitors/reports_2013/DTC_report_2013_Fovell.pdf).
- Fovell, R. G., Y. P. Bu, K. L. Corbosiero, W. w. Tung, Y. Cao, H.-C. Kuo, L.-H. Hsu, and H. Su, 2016: Influence of cloud microphysics and radiation on tropical cyclone structure and motion. *Meteor. Monog.*, **56**, 11.1–11.27, doi:10.1175/AMSMONOGRAPHS-D-15-0006.1.
- Fovell, R. G. and H. Su, 2007: Impact of cloud microphysics on hurricane track forecasts. *Geophys. Res. Lett.*, **134**, L24810, doi:10.1029/2007GL031723.
- Gopalakrishnan, S. G., F. D. Marks, J. A. Zhang, X. Zhang, J.-W. Bao, and V. Tallapragada, 2013: A study of the impacts of vertical diffusion on the structure and intensity of the tropical cyclones using the high-resolution HWRF system. *J. Atmos. Sci.*, **70**, 524–541.

- Hill, K. A. and G. M. Lackmann, 2009: Analysis of idealized tropical cyclone simulations using the Weather Research and Forecasting model: Sensitivity to turbulence parameterization and grid spacing. *Monthly Weather Review*, **137** (2), 745–765, doi:10.1175/2008MWR2220.1.
- Hong, S.-Y., 2010: A new stable boundary-layer mixing scheme and its impact on the simulated east asian summer monsoon. *Quart. J. Roy. Meteor. Soc.*, **136**, 1481–1496.
- Hong, S.-Y. and H.-L. Pan, 1996: Nonlocal boundary layer vertical diffusion in a medium-range forecast model. *Mon. Wea. Rev.*, **124**, 2322–2339, doi:10.1175/1520-0493(1996)124<2322:NBLVDI>2.0.CO;2.
- Hsu, L.-H., H.-C. Kuo, and R. G. Fovell, 2013: On the geographic asymmetry of typhoon translation speed across the mountainous island of Taiwan. *J. Atmos. Sci.*, **70**, 1006–1022, doi:10.1175/JAS-D-12-0173.1.
- Janjić, Z. I., 1994: The step-mountain Eta coordinate model: Further developments of the convection, viscous sublayer, and turbulence closure schemes. *Mon. Wea. Rev.*, **122**, 927–945, doi:10.1175/1520-0493(1994)122<0927:TSMECM>2.0.CO;2.
- Kepert, J. D., 2012: Choosing a boundary layer parameterization for tropical cyclone modeling. *Mon. Wea. Rev.*, **140**, 1427–1445, doi:10.1175/MWR-D-11-00217.1.
- Kepert, J. D., J. Schwendike, and H. Ramsay, 2016: Why is the tropical cyclone boundary layer not “well mixed”? *J. Atmos. Sci.*, **73**, 957–973, doi:10.1175/JAS-D-15-0216.1.
- Louis, J. F., 1979: A parametric model of vertical eddy fluxes in the atmosphere. *Bound.-Layer Meteor.*, **17**, 187–202.
- Mellor, G. L. and T. Yamada, 1974: A hierarchy of a turbulence closure models for planetary boundary layers. *J. Atmos. Sci.*, **31**, 1791–1806.
- Nakanishi, M. and H. Niino, 2004: An improved Mellor-Yamada Level-3 model with condensation physics: Its design and verification. *Bound.-Layer Meteor.*, **112**, 1–31, doi:10.1023/B:BOUN.0000020164.04146.98.
- Nava, O. A., R. G. Fovell, and L. F. Bosart, 2014: Impact of cloud-radiative processes on predecessor rain events. *31st Conf. on Hurricanes and Tropical Meteorology*, American Meteorological Society.
- Nolan, D. S., D. P. Stern, and J. A. Zhang, 2009a: Evaluation of planetary boundary layer parameterizations in tropical cyclones by comparison of in situ observations and high-resolution simulations of Hurricane Isabel (2003). Part II: Inner-core boundary layer and eyewall structure. *Monthly Weather Review*, **137** (11), 3675–3698, doi:10.1175/2009MWR2786.1.
- Nolan, D. S., J. A. Zhang, and D. P. Stern, 2009b: Evaluation of planetary boundary layer parameterizations in tropical cyclones by comparison of in situ observations and high-resolution

- simulations of Hurricane Isabel (2003). Part I: Initialization, maximum winds, and the outer-core boundary layer. *Monthly Weather Review*, **137** (11), 3651–3674, doi:10.1175/2009MWR2785.1.
- Smith, R. K. and G. L. Thomsen, 2010: Dependence of tropical-cyclone intensification on the boundary-layer representation in a numerical model. *Quart. J. Roy. Meteor. Soc.*, **136** (652), 1671–1685, doi:10.1002/qj.687.
- Troen, I. and L. Mahrt, 1986: A simple model of the atmospheric boundary layer; sensitivity to surface evaporation. *Bound.-Layer Meteor.*, **37**, 129–148.
- Vickers, D. and L. Mahrt, 2004: Evaluating formulations of stable boundary layer height. *J. Appl. Meteor.*, **43**, 1736–1749.
- Wang, W., J. A. Sippel, S. Abarca, L. Zhu, B. Liu, Z. Zhang, A. Mehra, and V. Tallapragada, 2018: Improving ncep hwrf simulations of surface wind and inflow angle in the eyewall area. *Wea. Forecasting*, **33**, 887–898, doi:10.1175/WAF-D-17-0115.1.
- Zhang, J. A., F. D. Marks, M. T. Montgomery, and S. Lorsolo, 2011a: An estimation of turbulent characteristics in the low-level region of intense hurricanes Allen (1980) and Hugo (1989). *Mon. Wea. Rev.*, **139**, 1447–1462.
- Zhang, J. A., R. F. Rogers, D. S. Nolan, and F. D. Marks, 2011b: On the characteristic height scales of the hurricane boundary layer. *Mon. Wea. Rev.*, **139**, 2523–2535.

## List of Figures

- 1 Scatterplots of  $K_m$  at 500 m MSL vs. wind speed (WS, m/s) at that level showing HWRf-generated mixing (grey dots) for experiments with  $\alpha = 1$ , compared to the observationally-derived estimates of Zhang et al. (2011a), indicated by “X” symbols. The  $K_m$ -WS relationship used in the Fovell-Bu cap is indicated (by red dashed line, labeled WS/0.6), along with observational  $K_m$  estimates that we subsequently removed. From Gopalakrishnan et al. (2013), with additions. 17
- 2 Vortex-following composite fields of temporally- and azimuthally-averaged eddy momentum mixing coefficient,  $K_m$ , from semi-idealized simulations made using the 2013 version of HWRf with Thompson microphysics and the GFS PBL scheme with varying values of  $\alpha$ . Also shown are simulations made using the “Capped  $K_m$ ” version of GFS and the YSU scheme with default and modified  $\text{Rib}_{cr}$  values. From Bu et al. (2017), with modifications and additions. 18
- 3 Radial profiles of temporally- and azimuthally-averaged 10-m wind speed from semi-idealized HWRf simulations using (a) GFS PBL runs using various values of  $\alpha$ ; and (b) the default and  $\text{Rib}_{cr} = 0.25$  YSU simulations [with GFS runs from (a) shown in grey for reference]. Modified from Bu et al. (2017). 19
- 4 Radius-height composites of temporally- and azimuthally-averaged radial (shaded) and tangential (grey contoured) winds, with radius nondimensionalized by the radius of maximum wind (RMW), for GFS/GFDL experiments varying  $\alpha$  from Bu et al. (2017). Thick black contour identifies the level at which inflow is equivalent to 10% of the maximum value, which has been used as a proxy for inflow layer depth by Zhang et al. (2011b) 20
- 5 Timeline of simulations (time in hours), indicating D3 cumulus deactivation time and analysis period. See text. 21
- 6 Time series of maximum 10-m wind (kts) every time step for (a) YSU and (b) MYNN simulations using longer (black) and shorter (red) physics time steps, controlled by the `nphs` switch. 22

- 7 As in Fig. 2, but for experiments using (a) GFS and (b) YSU varying the critical Richardson number  $Rib_{cr}$  from the schemes' respective default values. These simulations used the 2017 HWRF model (H217), GFS instead of GFSEDMF, and the YSU runs utilized its default surface layer scheme. 23
- 8 As in Fig. 4 but for H217 GFS/GFDL simulations using  $\alpha = 1$  and varying the critical Richardson number  $Rib_{cr}$ . Superimposed on the panels are rough estimates of inflow layer depth vs. radius from Zhang et al. (2011b) for all hurricanes (Cat. 1-5) and major storms (Cat. 4-5). 24
- 9 Similar to Figs. 4 and 8 but showing scaled inflow velocity (relative to maximum value in m/s reported at upper right of each panel) and eddy mixing applied to momentum ( $K_m$ , red  $20 \text{ m}^2/\text{s}$  contours) between 0 and 5 multiples of the RMW for H218 simulations using (a) GFSEDMF/GFDL uncapped ( $\alpha = 1$ ); (b) GFSEDMF/GFDL capped (operational version); (c) YSU/GFDL with default  $Rib_{cr} = 0.$ ; (d) YSU/GFDL with  $Rib_{cr} = 0.0125$ ; (e) MYJ/MYJSFC; and (f) MYNN/GFDL. 25
- 10 Scatterplots of  $K_m$  at 500 m MSL vs. wind speed at that level, computed using information between 1 and 5 multiples of the RMW, compared to a subset of observations from Zhang et al. (2011a). Red dots represent temporally- and azimuthally-averaged data, while grey dots are just temporally averaged. Shown are (a) GFSEDMF/GFDL uncapped ( $\alpha = 1$ ); (b) GFSEDMF/GFDL capped (operational version); (c) YSU/GFDL with default  $Rib_{cr} = 0.$ ; (d) YSU/GFDL with  $Rib_{cr} = 0.0125$ ; (e) MYJ/MYJSFC; and (f) MYNN/GFDL. 26
- 11 Composite analysis of radial wind velocity for Cat 4-5 storms normalized by the peak values as a function of altitude and radius normalized by RMW. The black line depicts the inflow layer height defined as where the radial wind speed is 10% of the peak inflow. The vertical profile of maximum inflow was constructed by taking the largest magnitude at each altitude between 1-2 multiples of the RMW, as indicated by the blue dashed line. From Zhang et al. (2011b). 27

- 12 Vertical profiles of maximum radial inflow, based on temporally- and azimuthally-averaged winds, for HWRF H218 simulations using (a) GFSEDMF/GFDL (with and without capping); (b) YSU/GFDL (default and  $\text{Rib}_{cr} = 0.0125$ ); (c) MYJ/MYJSFC; and (d) MYNN/GFDL. Black curve represents data from Zhang et al. (2011b), obtained as described in the text. On each successive panel, previously introduced profiles are retained (as thin curves) for reference. 28
- 13 As in Fig. 3 but for H218 runs with MYNN (black), GFSEDMF capped (red), and GFSEDMF uncapped (blue). All simulations use the GFDL surface layer scheme. Large dots mark 34-kt wind radii. 29
- 14 Vertical cross-sections of radial (shaded) and tangential (blue 10 m/s contours) for simulations using (a) capped GFSEDMF/GFDL; and (b) MYNN/GFDL. 30
- 15 Vertical cross-sections of (at top) water vapor mixing ratio (shaded) and eddy mixing ( $20 \text{ m}^2/\text{s}$  contours) applied to scalars ( $K_h$ ) for (a) GFSEDMF/GFDL, and (b) MYNN/GFDL, and (at bottom) the GFSEDMF-MYNN difference fields for vapor (shaded) and mixing ( $10 \text{ m}^2/\text{s}$  contours). 31
- 16 Vertically averaged vertical velocity between the surface and 500 mb levels (shaded) for (a) GFSEDMF/GFDL capped, and (b) MYNN/GFDL. 32

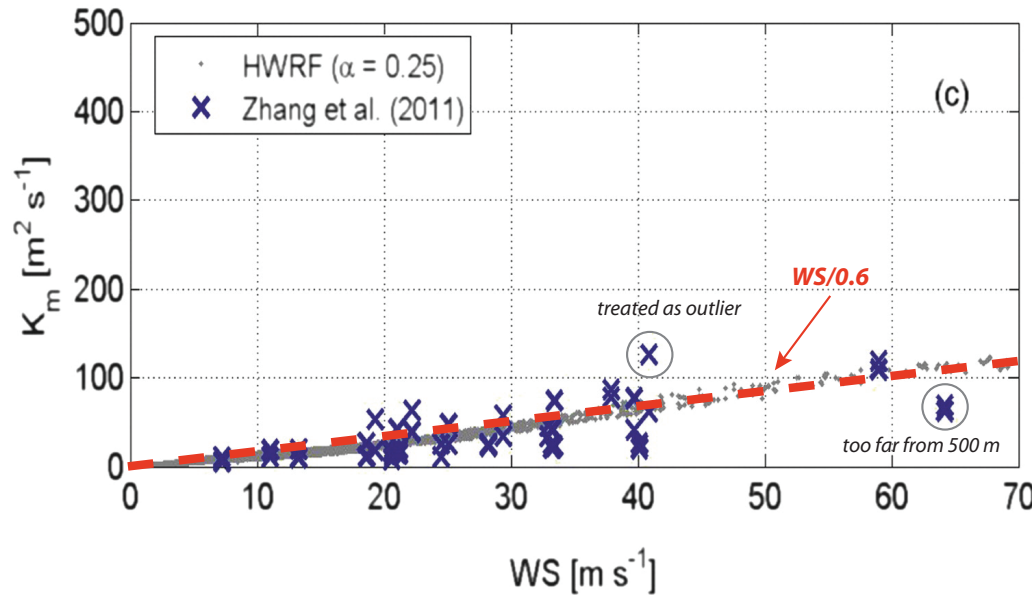


FIG. 1. Scatterplots of  $K_m$  at 500 m MSL vs. wind speed (WS, m/s) at that level showing HWRP-generated mixing (grey dots) for experiments with  $\alpha = 1$ , compared to the observationally-derived estimates of Zhang et al. (2011a), indicated by “X” symbols. The  $K_m$ -WS relationship used in the Fovell-Bu cap is indicated (by red dashed line, labeled WS/0.6), along with observational  $K_m$  estimates that we subsequently removed. From Gopalakrishnan et al. (2013), with additions.

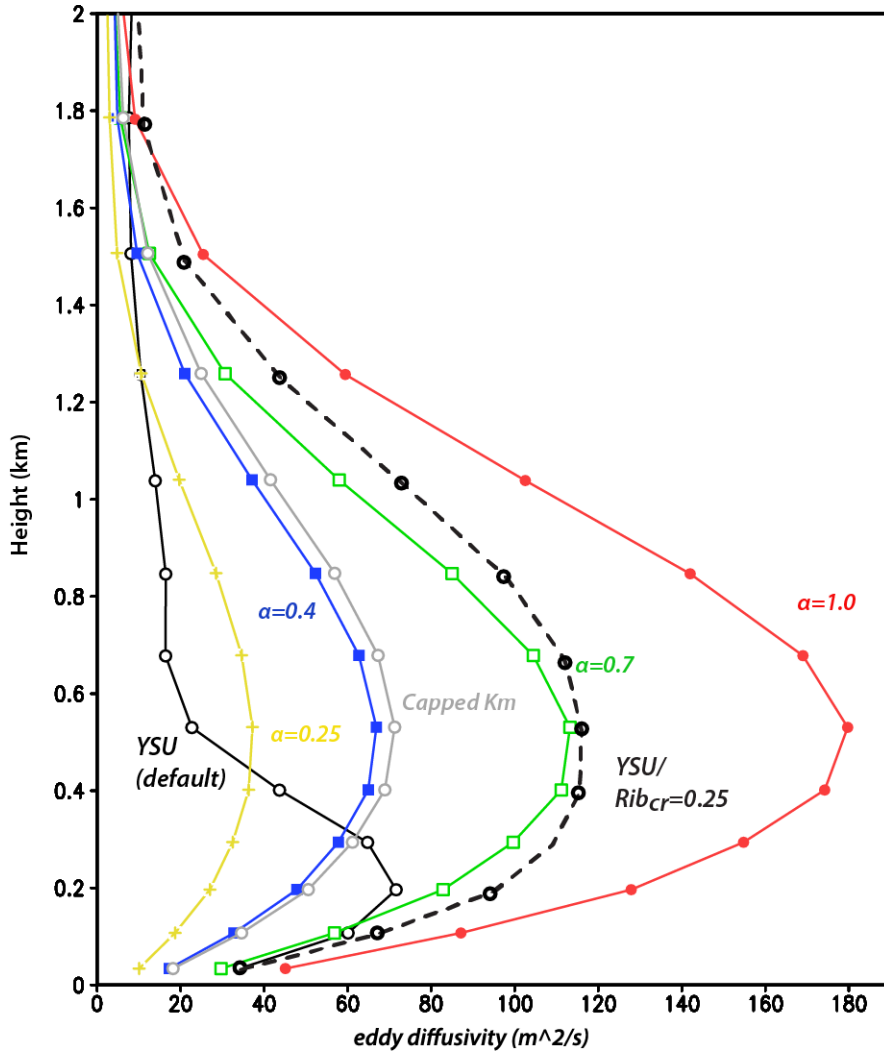


FIG. 2. Vortex-following composite fields of temporally- and azimuthally-averaged eddy momentum mixing coefficient,  $K_m$ , from semi-idealized simulations made using the 2013 version of HWRF with Thompson microphysics and the GFS PBL scheme with varying values of  $\alpha$ . Also shown are simulations made using the “Capped  $K_m$ ” version of GFS and the YSU scheme with default and modified  $Rib_{cr}$  values. From Bu et al. (2017), with modifications and additions.

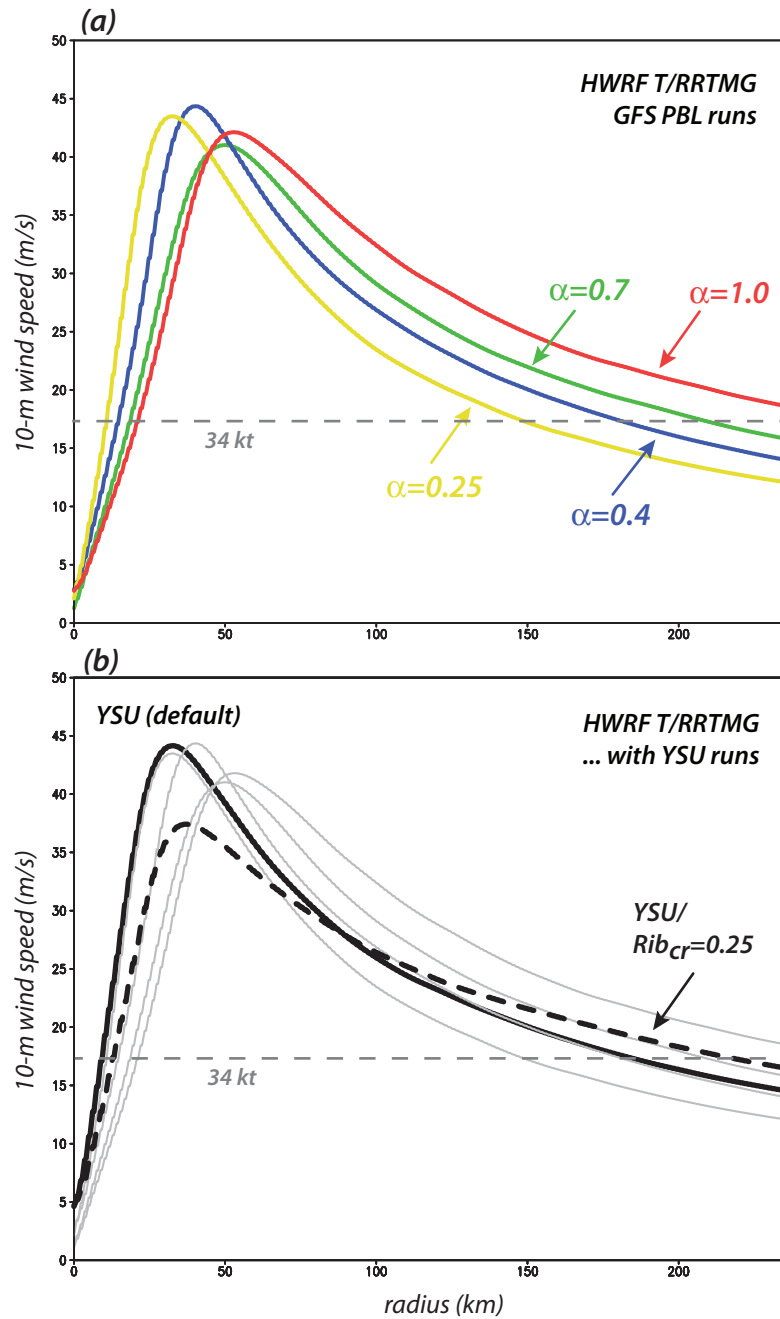


FIG. 3. Radial profiles of temporally- and azimuthally-averaged 10-m wind speed from semi-idealized HWRf simulations using (a) GFS PBL runs using various values of  $\alpha$ ; and (b) the default and  $Rib_{cr} = 0.25$  YSU simulations [with GFS runs from (a) shown in grey for reference]. Modified from Bu et al. (2017).

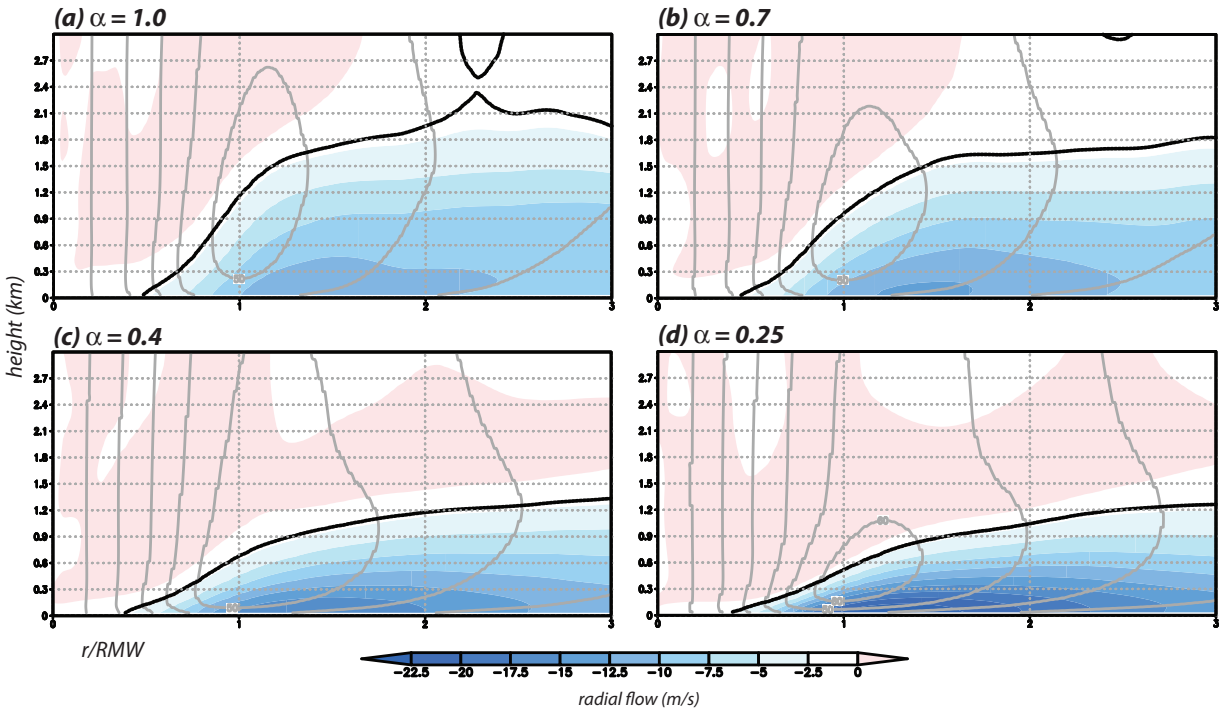


FIG. 4. Radius-height composites of temporally- and azimuthally-averaged radial (shaded) and tangential (grey contoured) winds, with radius nondimensionalized by the radius of maximum wind (RMW), for GFS/GFDL experiments varying  $\alpha$  from Bu et al. (2017). Thick black contour identifies the level at which inflow is equivalent to 10% of the maximum value, which has been used as a proxy for inflow layer depth by Zhang et al. (2011b)

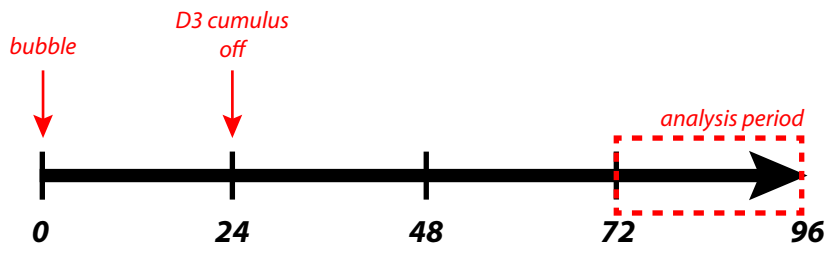


FIG. 5. Timeline of simulations (time in hours), indicating D3 cumulus deactivation time and analysis period. See text.

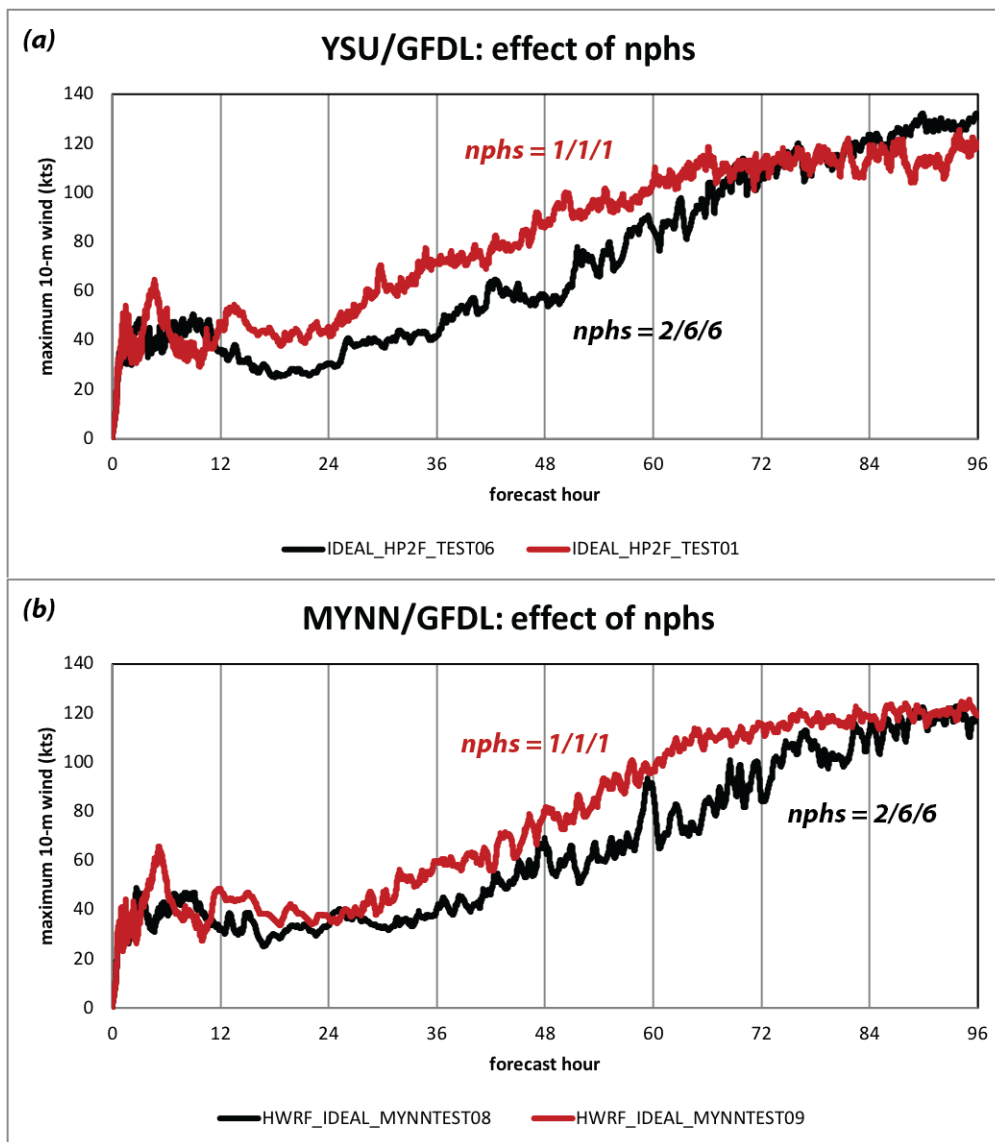


FIG. 6. Time series of maximum 10-m wind (kts) every time step for (a) YSU and (b) MYNN simulations using longer (black) and shorter (red) physics time steps, controlled by the `nphs` switch.

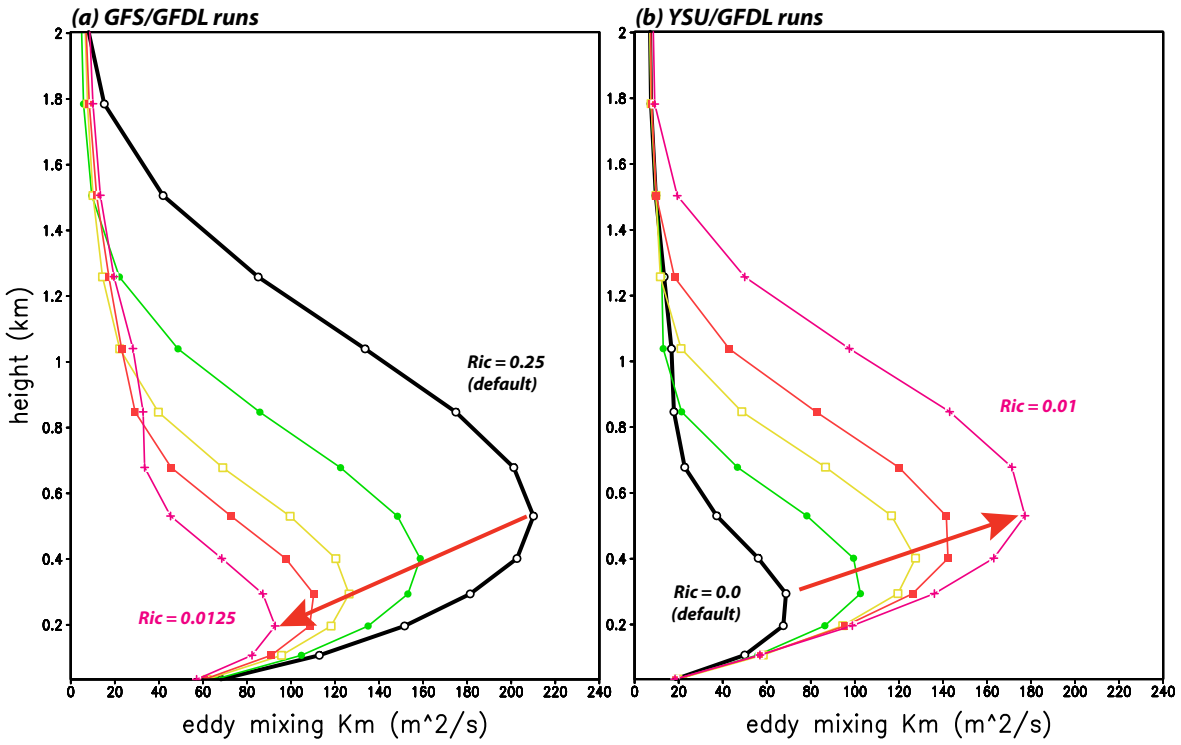


FIG. 7. As in Fig. 2, but for experiments using (a) GFS and (b) YSU varying the critical Richardson number  $Ric_{cr}$  from the schemes' respective default values. These simulations used the 2017 HWRF model (H217), GFS instead of GFSEDMF, and the YSU runs utilized its default surface layer scheme.

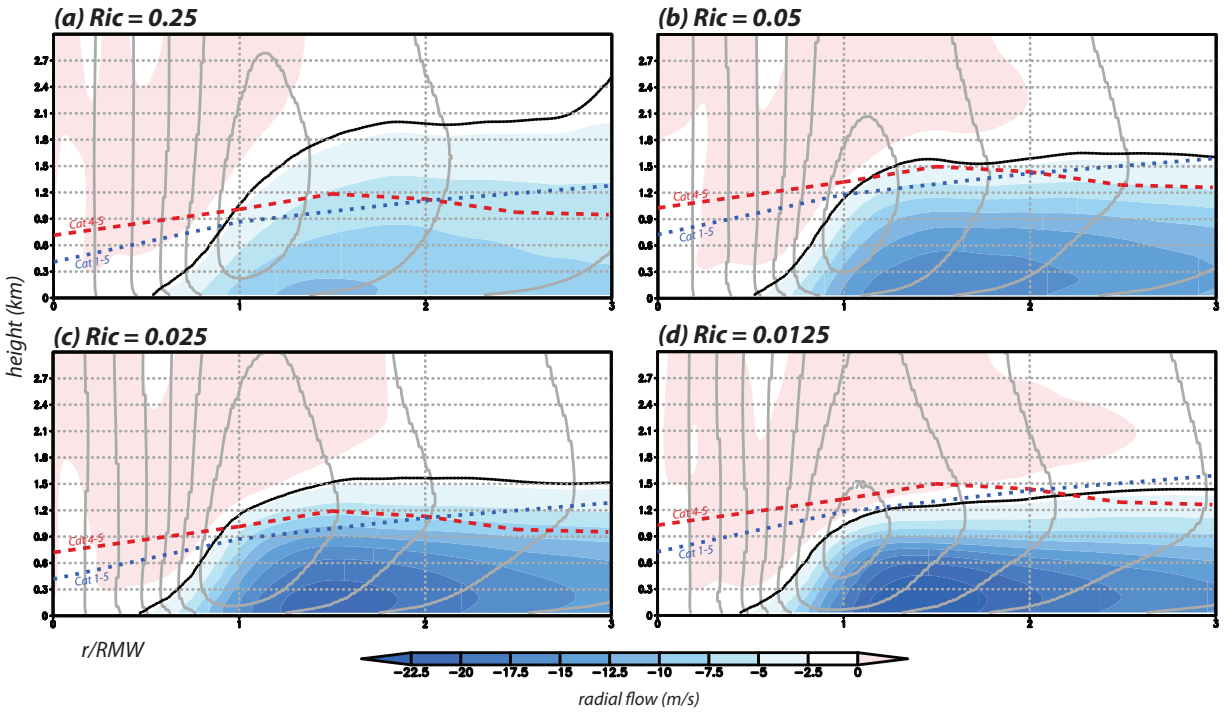


FIG. 8. As in Fig. 4 but for H217 GFS/GFDL simulations using  $\alpha = 1$  and varying the critical Richardson number  $Ric_{cr}$ . Superimposed on the panels are rough estimates of inflow layer depth vs. radius from Zhang et al. (2011b) for all hurricanes (Cat. 1-5) and major storms (Cat. 4-5).

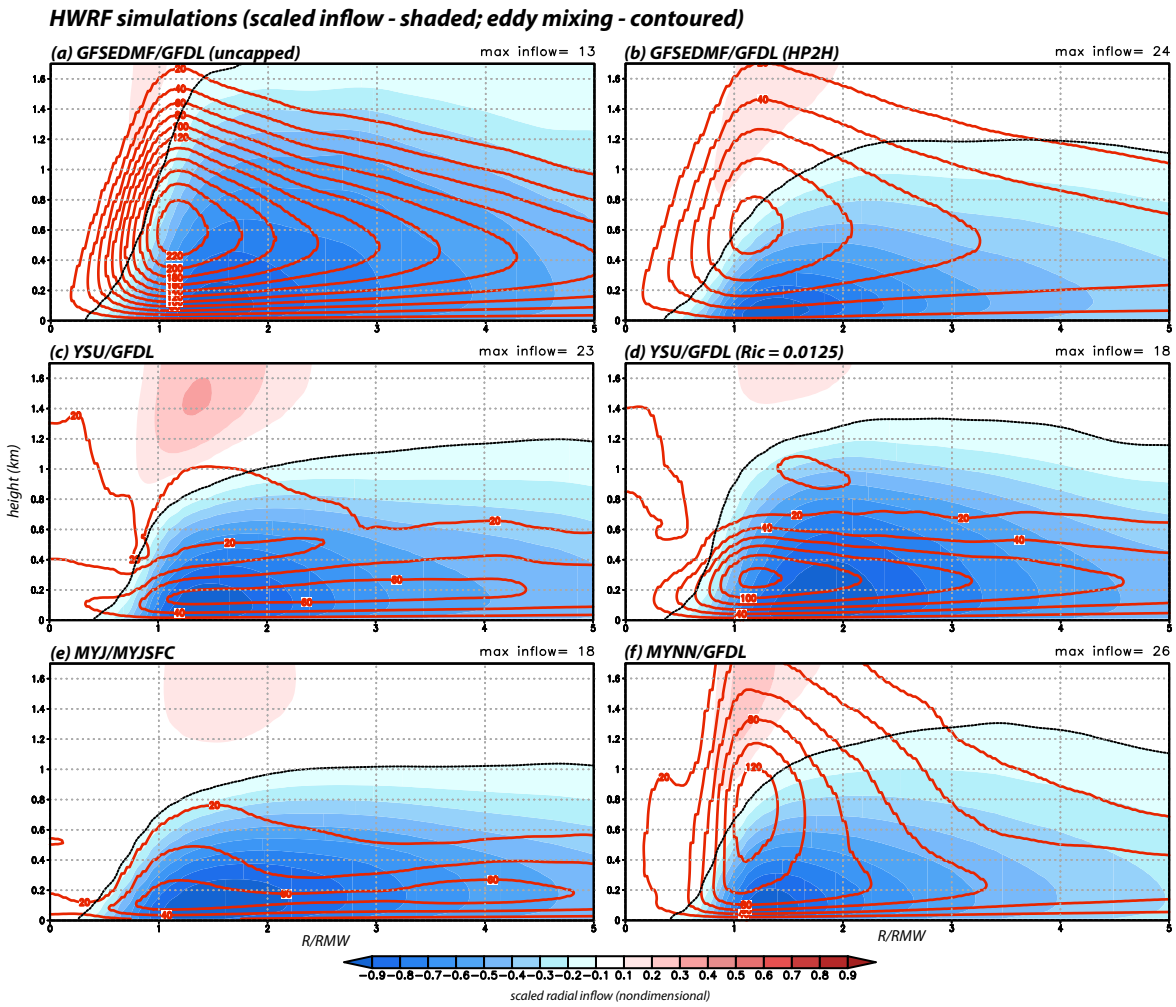


FIG. 9. Similar to Figs. 4 and 8 but showing scaled inflow velocity (relative to maximum value in m/s reported at upper right of each panel) and eddy mixing applied to momentum ( $K_m$ , red  $20 \text{ m}^2/\text{s}$  contours) between 0 and 5 multiples of the RMW for H218 simulations using (a) GFSEDMF/GFDL uncapped ( $\alpha = 1$ ); (b) GFSEDMF/GFDL capped (operational version); (c) YSU/GFDL with default  $\text{Rib}_{cr} = 0$ ; (d) YSU/GFDL with  $\text{Rib}_{cr} = 0.0125$ ; (e) MYJ/MYJSFC; and (f) MYNN/GFDL.

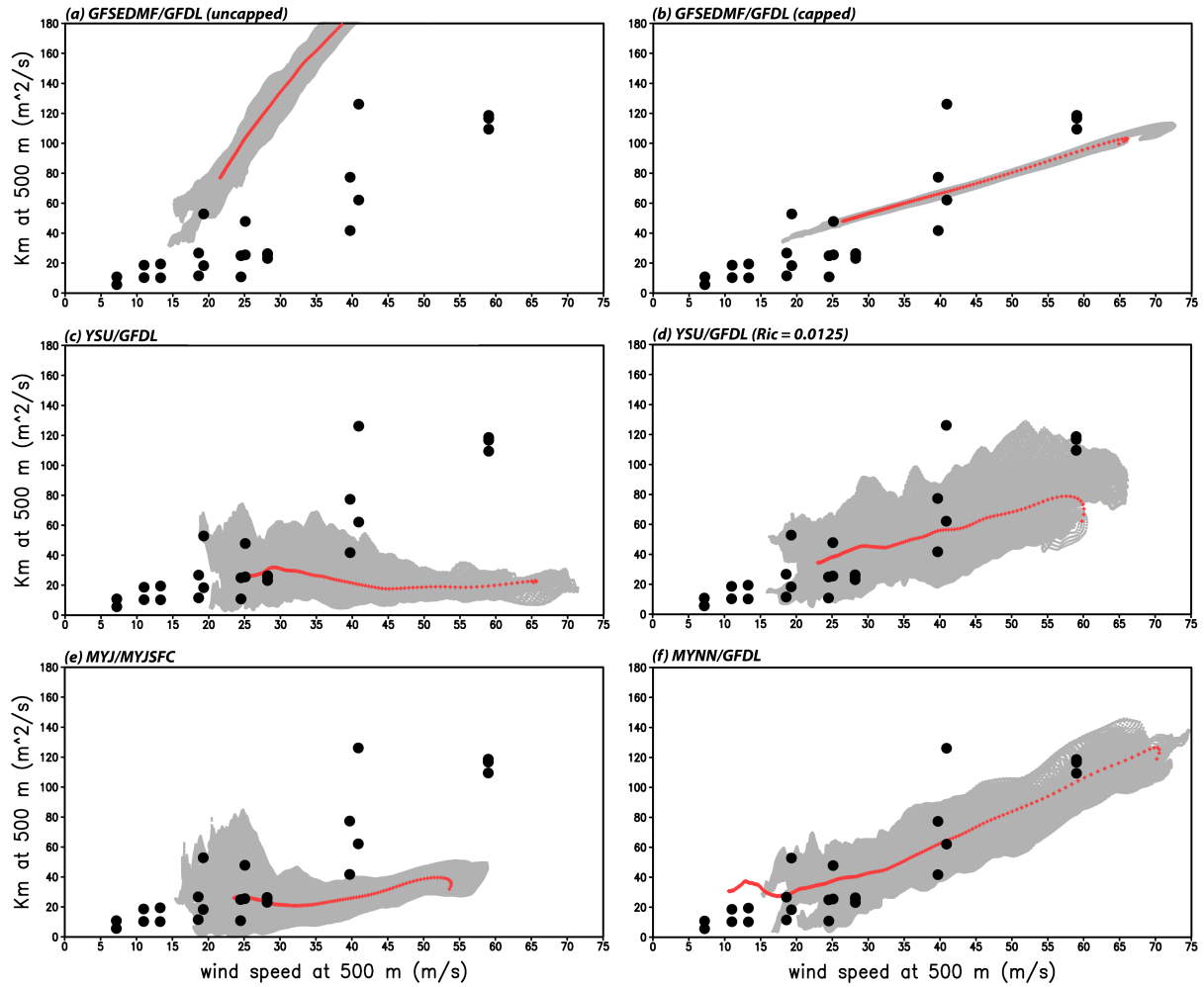


FIG. 10. Scatterplots of  $K_m$  at 500 m MSL vs. wind speed at that level, computed using information between 1 and 5 multiples of the RMW, compared to a subset of observations from Zhang et al. (2011a). Red dots represent temporally- and azimuthally-averaged data, while grey dots are just temporally averaged. Shown are (a) GFSEDMF/GFDL uncapped ( $\alpha = 1$ ); (b) GFSEDMF/GFDL capped (operational version); (c) YSU/GFDL with default  $Rib_{cr} = 0.$ ; (d) YSU/GFDL with  $Rib_{cr} = 0.0125$ ; (e) MYJ/MYJSFC; and (f) MYNN/GFDL.

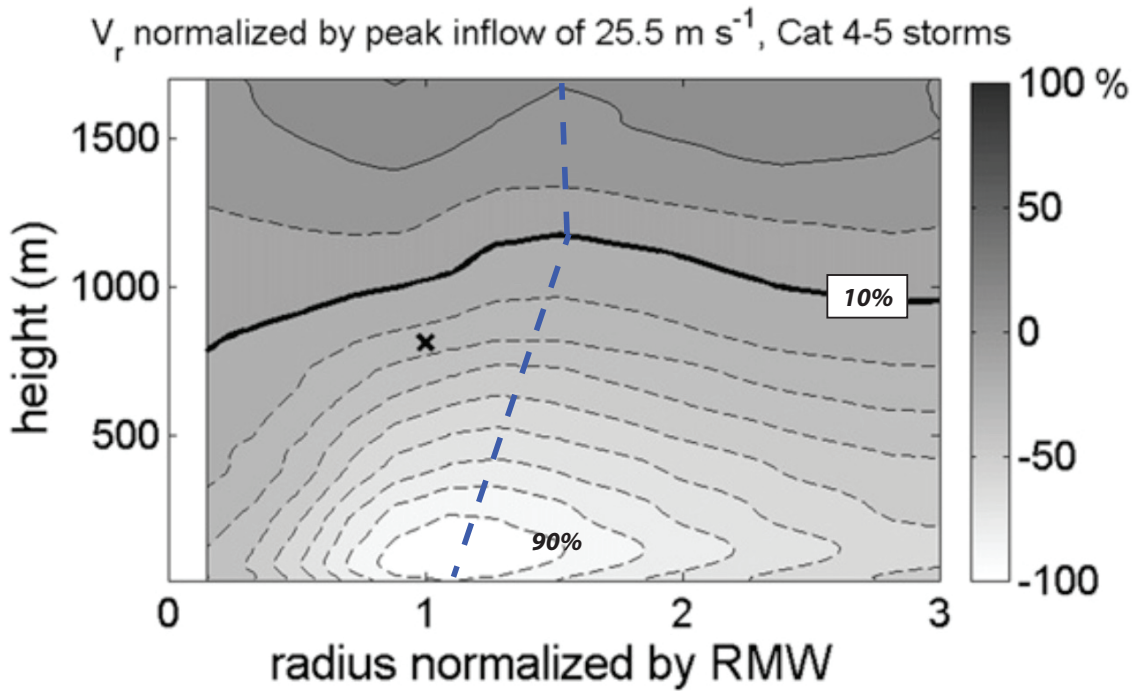


FIG. 11. Composite analysis of radial wind velocity for Cat 4-5 storms normalized by the peak values as a function of altitude and radius normalized by RMW. The black line depicts the inflow layer height defined as where the radial wind speed is 10% of the peak inflow. The vertical profile of maximum inflow was constructed by taking the largest magnitude at each altitude between 1-2 multiples of the RMW, as indicated by the blue dashed line. From Zhang et al. (2011b).

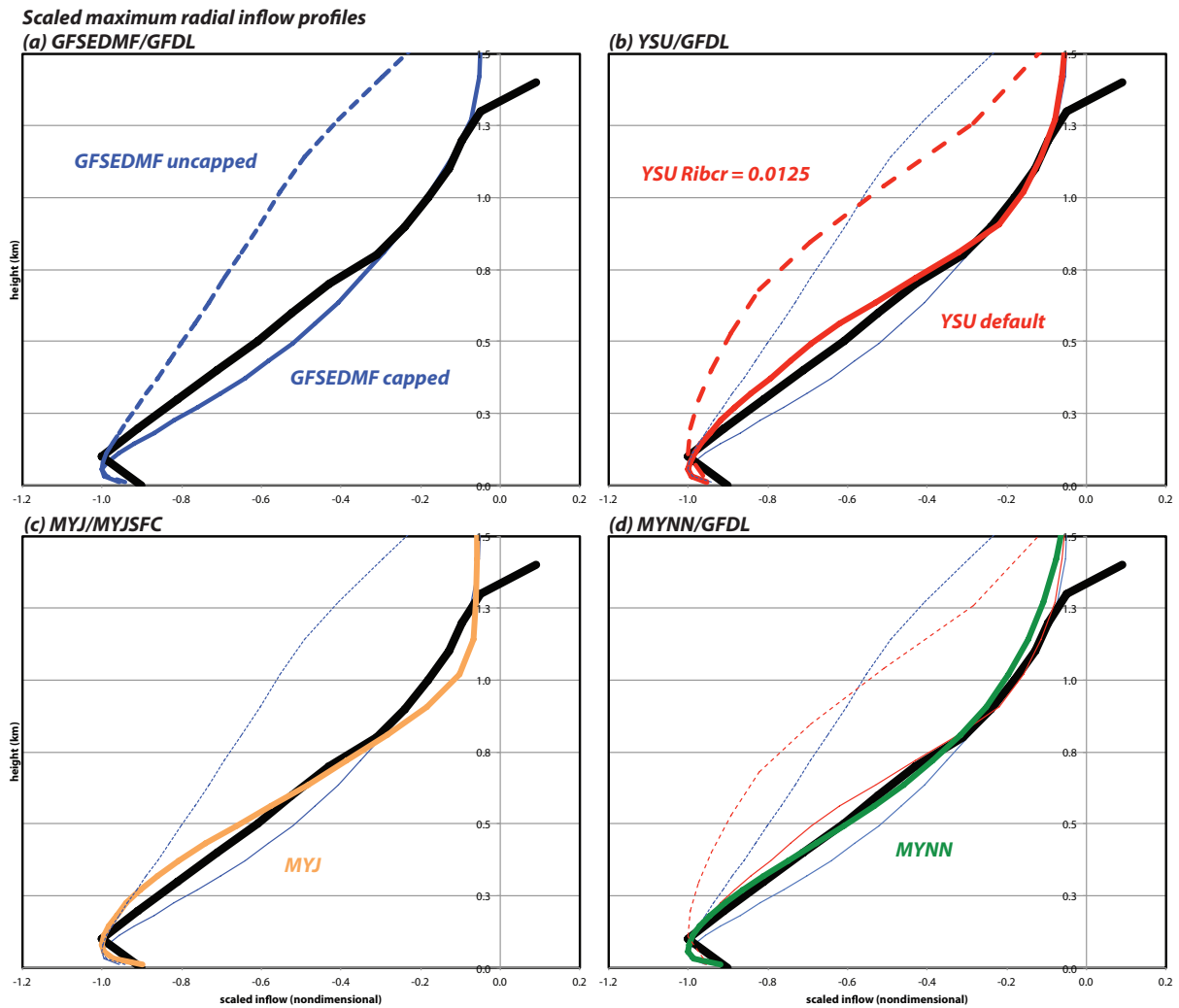


FIG. 12. Vertical profiles of maximum radial inflow, based on temporally- and azimuthally-averaged winds, for HWRF H218 simulations using (a) GFSEDMF/GFDL (with and without capping); (b) YSU/GFDL (default and  $Rib_{cr} = 0.0125$ ); (c) MYJ/MYJSFC; and (d) MYNN/GFDL. Black curve represents data from Zhang et al. (2011b), obtained as described in the text. On each successive panel, previously introduced profiles are retained (as thin curves) for reference, and only newly introduced information is labeled.

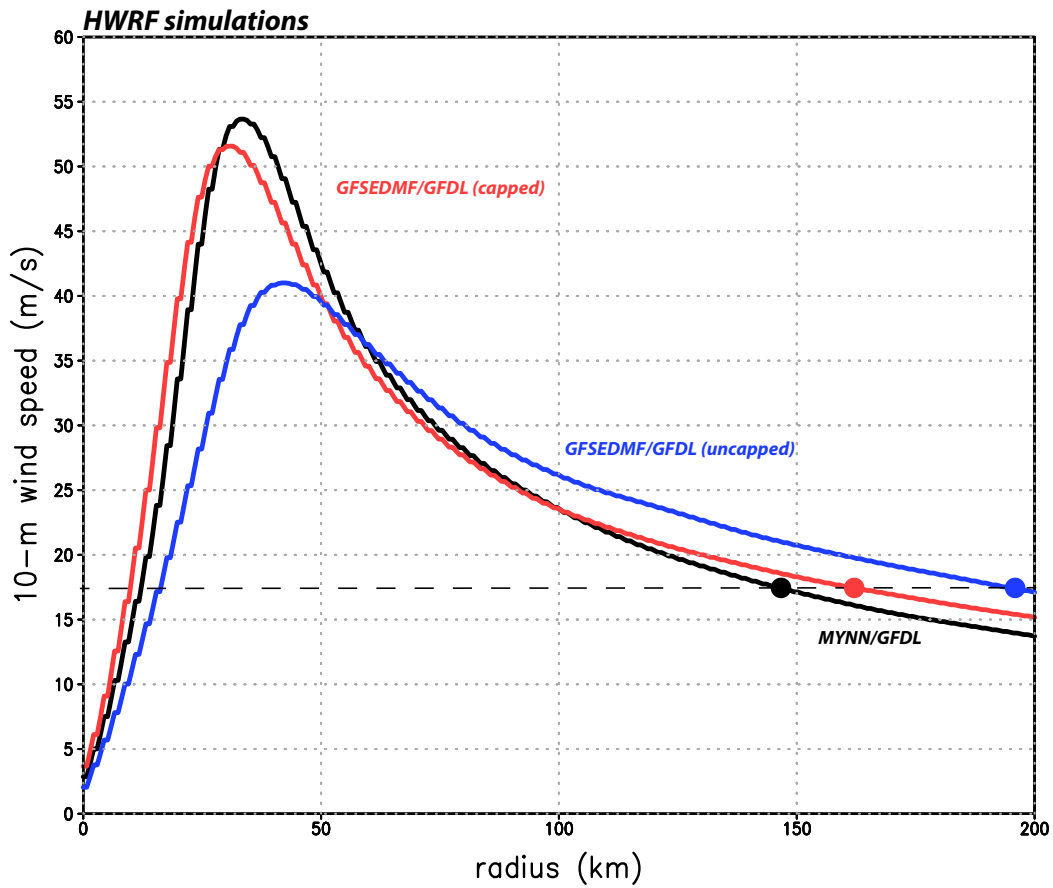


FIG. 13. As in Fig. 3 but for H218 runs with MYNN (black), GFSEDMF capped (red), and GFSEDMF uncapped (blue). All simulations use the GFDL surface layer scheme. Large dots mark 34-kt wind radii.

**HWRF simulations (radial wind - shaded; tangential wind - contoured)**

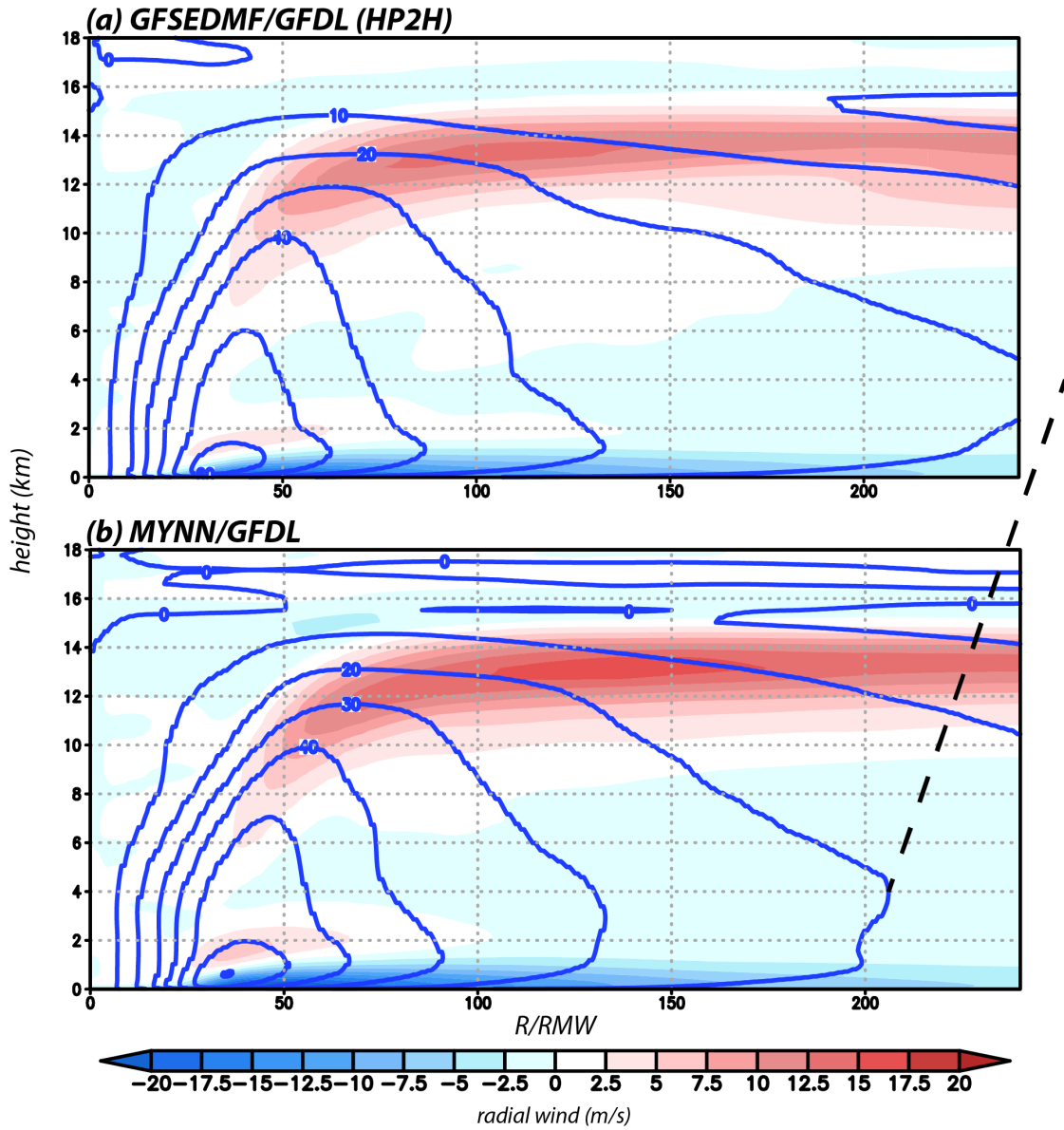


FIG. 14. Vertical cross-sections of radial (shaded) and tangential (blue 10 m/s contours) for simulations using (a) capped GFSEDMF/GFDL; and (b) MYNN/GFDL.

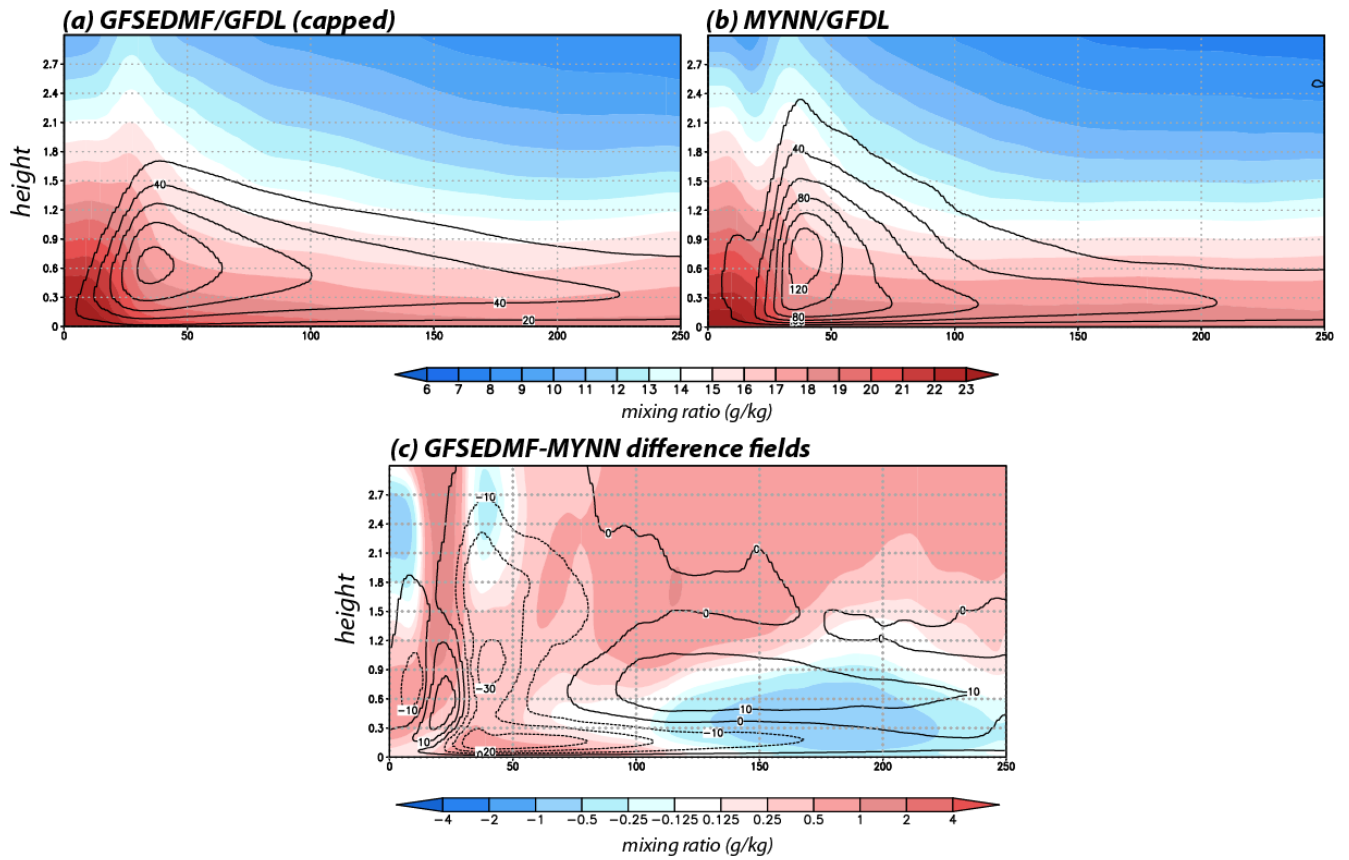


FIG. 15. Vertical cross-sections of (at top) water vapor mixing ratio (shaded) and eddy mixing ( $20 \text{ m}^2/\text{s}$  contours) applied to scalars ( $K_h$ ) for (a) GFSEDMF/GFDL, and (b) MYNN/GFDL, and (at bottom) the GFSEDMF-MYNN difference fields for vapor (shaded) and mixing ( $10 \text{ m}^2/\text{s}$  contours).

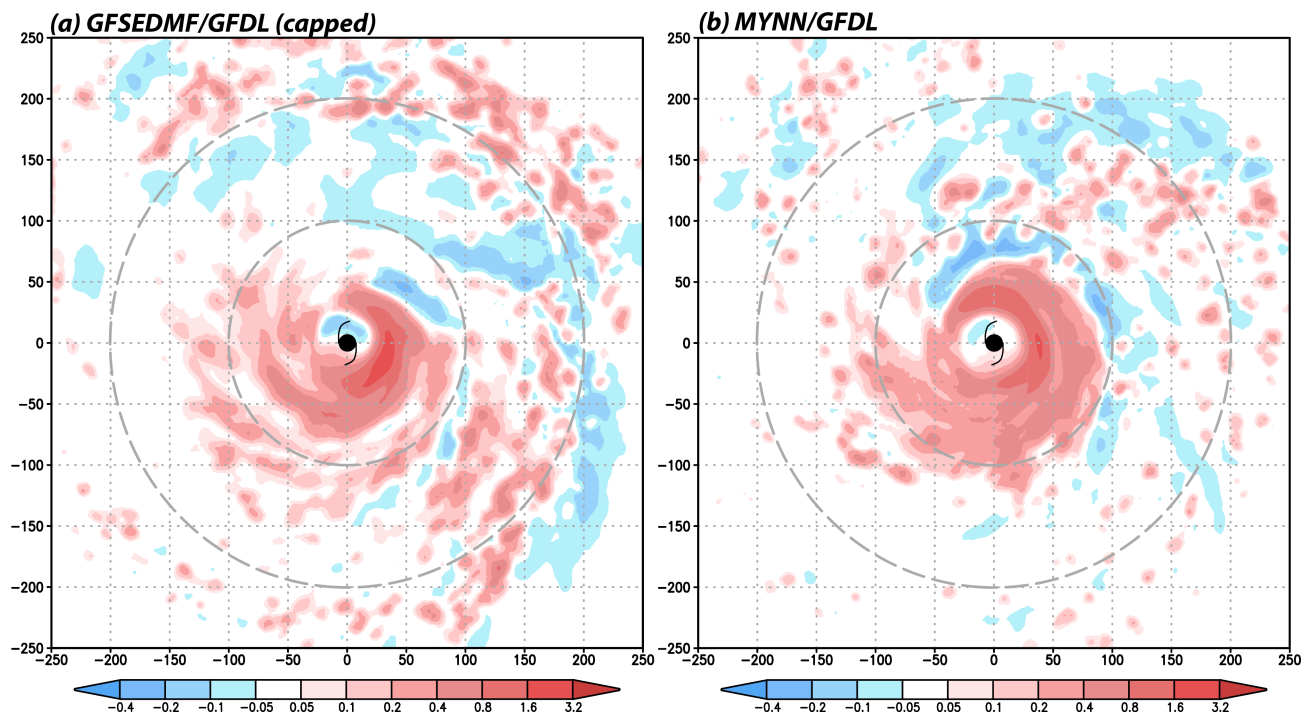


FIG. 16. Vertically averaged vertical velocity between the surface and 500 mb levels (shaded) for (a) GFSEDMF/GFDL capped, and (b) MYNN/GFDL.